Astron. Astrophys. 328, 617–627 (1997)

ASTRONOMY
AND
ASTROPHYSICS

Chemistry and rotational excitation of O_2 in interstellar clouds

II. The $^{16}O^{18}O$ isotopomer⋆

P. Maréchal, Y.P. Viala, and L. Pagani

DEMIRM, Observatoire de Paris, 61 Av. de l'Observatoire, F-75014 Paris, France

Received 15 January 1997 / Accepted 9 June 1997

Abstract. Although molecular oxygen O_2 is predicted to be an important constituent of the interstellar gas, it has not yet been observed in Galactic interstellar clouds. While ongoing O_2 observation projects in our Galaxy have to use stratospheric balloons or satellites, several teams have already tried to observe its isotopomer $^{16}O^{18}O$ with ground-based telescopes. In this paper, a chemical model of interstellar clouds including ^{18}O and ^{13}C isotopic reactions with a non-LTE calculation of $^{16}O^{18}O$ rotational population has been used to predict the intensity of the 3 $^{16}O^{18}O$ lines observable from the ground, namely the 234, 298 and 402 GHz lines. These predictions are compared to the upper limits obtained by Maréchal et al. (1997a) and to the tentative detection obtained by Pagani et al. (1993) towards L134N. We show that only the 234 GHz line is observable with today's receivers and that the strong upper limits we have reported are not compatible with a standard steady-state model. Clumpiness, high (0.7) C/O ratio or other non-standard models are required to explain our observations. The consequence of the ^{18}O isotopic fractionation is also discussed.

Key words: molecular processes – ISM: abundances, molecules – radio lines: ISM

1. Introduction

Oxygen is the most abundant element in the universe after hydrogen and helium and thus plays an important role in the chemistry of interstellar clouds. Since the first chemical models of interstellar clouds dealing with the simplest molecules and assuming steady-state chemical equilibrium (Herbst & Klemperer 1973, Viala & Walmsley 1976), it has been recognized, and confirmed by more recent models, that molecular oxygen O_2 should have an abundance comparable to that of CO deep inside the clouds. It must be however noted that a whole series of special models show a dramatic drop in O_2 abundance in many situations. This is for instance the case in early stages of time dependent models (e.g. Millar et al. 1996), in models in which turbulent mixing occurs between the envelope and the core of the clouds (e.g. Chièze & Pineau des Forêts 1989), in the high ionization phase of models exhibiting two stable chemical phases (e.g. Le Bourlot et al. 1995) and in clouds showing a very highly clumpy structure (Spaans 1996, private communication). Thus the observation of molecular oxygen to measure its abundance should allow us to test the interstellar chemical models and to give some insight on the total amount of gas phase oxygen in molecular clouds.

Due to the presence of a large quantity of O_2 in the terrestrial atmosphere, detection of $^{16}O_2$ in our Galaxy requires the launch of balloon- or satellite-borne heterodyne receivers. There are however two possibilities to try to detect O_2 from the ground by getting rid of the opacity due to the atmospheric lines. The first one consists in observing extragalactic sources with redshift large enough for the lines to sit far away in the wings of the atmospheric lines. Several attempts have been made towards such extragalactic sources (e.g. Combes et al. 1991, Combes & Wiklind 1995), all leading to negative results. The second way is to detect its ^{18}O-substituted isotopomer. Indeed, lines connecting even N levels of $^{16}O^{18}O$ do not exist for the main $^{16}O_2$ isotope and are consequently not blocked by atmospheric lines. Several attempts to observe the $^{16}O^{18}O$ (N, J): (2, 1)–(0, 1) line at 234 GHz have been led without success (Goldsmith et al. 1985, Liszt & Vanden Bout 1985, Combes et al. 1991, Fuente et al. 1993, Maréchal et al. 1997a, hereafter MPLC), apart from one possible case in L134N for which a 3σ tentative detection has been reported (Pagani et al. 1993). In some of the sources for which $^{16}O^{18}O$ has not been detected, our observations have permitted to establish the lowest upper limits of the $^{16}O^{18}O/C^{18}O$ ratio obtained up to now for galactic sources, which really begin to be in contradiction with standard chemical model predictions (MPLC).

The main purpose of this paper is to make theoretical predictions of the emissivities of the $^{16}O^{18}O$ lines accessible from

Send offprint requests to: Y. Viala (viala@obspm.fr)

Table 4 only available in electronic form at the CDS (Strasbourg) via anonymous ftp to cdsarc.u-strasbg.fr (130.79.128.5) or via http://cdsweb.u-strasbg.fr/Abstract.html

the ground and to interpret the low upper limits of the $^{16}O^{18}O$ column densities deduced from the observations. To do this, in the same way as we have computed the O_2 abundance and the emissivities of its rotational lines (Paper I: Maréchal et al. 1997b, hereafter MVB), the processes of radiative and collisional transfer between the rotational levels of $^{16}O^{18}O$ have been included in a steady-state model which works out chemical and thermal balances in molecular clouds. The paper is organized as follows : the determination of the spectroscopic parameters of $^{16}O^{18}O$ in its ground vibrational level needed to compute its rotational population is presented in Sect. 2, together with a brief description of its chemistry. The emissivities of $^{16}O^{18}O$ lines computed for various cloud parameters such as the total visual extinction, the density, the ultraviolet radiation field or the C/O elemental ratio are presented in Sect. 3. The interpretation of the observations is done in Sect. 4. The isotopic fractionation of the oxygen-bearing species has also been investigated and is presented in Sect. 5. Sect. 6 summarizes our main conclusions.

2. The chemistry and spectroscopy of $^{16}O^{18}O$

2.1. The chemistry

The chemical reaction scheme involving isotopic substituted ^{13}C- and ^{18}O- molecules is merely obtained by duplicating the reactions between C- and O- bearing species and replacing the main isotopes by ^{13}C and ^{18}O. Four isotopic exchange reactions have also been included in the model (Langer et al. 1984) and we consider both forward and backward reactions:

$$\begin{array}{lll} ^{13}C^+ + {}^{12}CO & \longleftrightarrow {}^{12}C^+ + {}^{13}CO & (\Delta E = 35\ K) \\ H^{12}CO^+ + {}^{13}CO & \longleftrightarrow H^{13}CO^+ + {}^{12}CO & (\Delta E = 9\ K) \\ HC^{16}O^+ + C^{18}O & \longleftrightarrow HC^{18}O^+ + C^{16}O & (\Delta E = 14\ K) \\ H^{13}C^{16}O^+ + {}^{12}C^{18}O & \longleftrightarrow H^{12}C^{18}O^+ + {}^{13}C^{16}O & (\Delta E = 5\ K) \end{array} \quad (1)$$

The library of reactions contains about 2100 reactions among 111 chemical species. As in MVB, it is extracted from Viala (1986) where only C and O compounds have been kept; rate coefficients have been up-dated according to the compilations by Anicich (1993) for ion-neutral reactions and by Millar et al. (1996) for neutral-neutral reactions.

The molecule $^{16}O^{18}O$ is mainly produced through two neutral-neutral reactions, instead of only one for $^{16}O_2$:

$$\begin{array}{l} ^{18}O + {}^{16}OH \rightarrow {}^{16}O^{18}O + H \\ ^{16}O + {}^{18}OH \rightarrow {}^{16}O^{18}O + H \end{array} \quad (2)$$

with both reaction rates assumed equal to that of the corresponding reaction involving the principal isotope ^{16}O, i.e. $k = 3.3\ 10^{-10} T^{-0.4} \exp(-6.0/T)$ $cm^3 s^{-1}$ (Davidsson & Stenholm 1990).

Photoionisation and photodissociation by UV photons are very efficient destruction processes of $^{16}O^{18}O$. In the regions where UV is excluded, $^{16}O^{18}O$ is mainly destroyed by reactive collisions with C^+, He^+ and H^+, like $^{16}O_2$.

Table 1. Spectroscopic constants for the ground vibrational level of $^{16}O^{18}O$ (Gordy & Cook 1984)

	MHz
B	40,707.408
D	0.129
λ_0	59,499.097
λ_1	0.05312
γ_0	-238.4888
γ_1	-0.000619

The $^{16}O^{18}O$ formation rate is twice more efficient than that of $^{16}O_2$ so that one can expect the $^{16}O_2/^{16}O^{18}O$ ratio to be equal to half the isotopic ratio $[^{16}O]/[^{18}O]$ (=500). The isotopic ratio of the other oxygen-bearing species $X^{16}O/X^{18}O$ can differ from the isotopic elemental ratio due to the isotopic exchange reactions and the selective photodissociation of CO and $C^{18}O$. This is discussed in Sect. 5 below.

2.2. The spectroscopy

To determine the rotational population of $^{16}O^{18}O$, we take into account the following processes: spontaneous emission, stimulated emission and absorption of the ambient background radiation and collisional excitation and de-excitation between the first 46 rotational levels of $^{16}O^{18}O$ ($E_{max} \sim 500$ K).

As O_2, $^{16}O^{18}O$ is a $^3\Sigma$ molecule. It however contains two different atoms, so that, contrarily to $^{16}O_2$, even N levels do exist (except the level N=J=0 which is forbidden for symmetry reasons). The energies of the levels are obtained from the same set of equations that was used for $^{16}O_2$ (eqs. (2)–(3) in MVB) with the spectroscopic constants listed in Table 1.

The electric dipole moment of $^{16}O^{18}O$ is too small to be taken into account and we consider only radiative magnetic dipole transitions between the rotational levels which obey to the selection rules: $\Delta N = 0, \pm 2$ and $\Delta J = 0, \pm 1$. For all transitions considered in the model, the upper level energies, the frequencies and the Einstein coefficients are listed in Table 2 and are obtained by using equations (5)–(7) of MVB and the line strengths listed in Table XIII of Steinbach's thesis (1974).

The excitation and de-excitation of $^{16}O^{18}O$ by collision with H_2 and He are considered for ΔN=0, 1, 2, 3, 4, 5 and 6 using the collision rates of $^{16}O_2$ (Corey 1984, Orlikowsky 1986, Corey et al. 1986). Collision rates for transitions with odd values of ΔN and for levels with even values of N which do not exist for O_2, have been obtained by interpolation, as explained in Appendix 1 where the de-excitation rates of $^{16}O^{18}O$–He are listed (Table 4).

3. The most intense rotational lines of $^{16}O^{18}O$

In all model calculations presented hereafter, the clouds are assumed to be homogeneous and submitted to the interstellar UV radiation field of Mathis et al. (1983) with a possible scaling factor constant over the range 913–4000 Å. For the elemental abundances, we adopted the solar values from the compilation of Anders & Grevesse (1989) with the same depletion factor

Table 2. Upper level energies, frequencies and spontaneous emission coefficients of the first 71 rotational lines of $^{16}O^{18}O$

$(N, J)\rightarrow(N', J')$	Upper level energy (K)	ν (MHz)	A (s^{-1})	$(N, J)\rightarrow(N', J')$	Upper level energy (K)	ν (MHz)	A (s^{-1})
(1, 1)→(1, 2)	6.51	56722.05	$5.57\ 10^{-10}$	(9, 8)→(7, 7)	175.61	1325107	$1.50\ 10^{-8}$
(1, 1)→(1, 0)		118759.9	$4.47\ 10^{-9}$	(9, 8)→(7, 8)		1385568	$7.84\ 10^{-8}$
(2, 1)→(0, 1)	11.23	233946.2	$1.33\ 10^{-8}$	(9, 9)→(7, 8)	178.41	1443874	$2.20\ 10^{-8}$
(2, 2)→(0, 1)	14.33	298473.2	$5.86\ 10^{-9}$	(9, 9)→(9, 10)		61121.94	$9.07\ 10^{-10}$
(2, 2)→(2, 3)		57899.98	$7.17\ 10^{-10}$	(9, 9)→(9, 8)		58305.92	$7.87\ 10^{-10}$
(2, 2)→(2, 1)		64526.97	$9.08\ 10^{-10}$	(10, 9)→(8, 8)	214.68	1488023	$1.74\ 10^{-8}$
(3, 2)→(1, 1)	23.07	345017.9	$1.77\ 10^{-9}$	(10, 9)→(8, 9)		1548824	$8.85\ 10^{-8}$
(3, 2)→(1, 2)		401739.9	$2.28\ 10^{-8}$	(10, 10)→(8, 9)	217.46	1606792	$2.46\ 10^{-8}$
(3, 3)→(1, 2)	26.04	463778.4	$8.18\ 10^{-9}$	(10, 10)→(10, 11)		61428.70	$9.22\ 10^{-10}$
(3, 3)→(3, 4)		58656.39	$7.73\ 10^{-10}$	(10, 10)→(10, 9)		57968.04	$7.74\ 10^{-10}$
(3, 3)→(3, 2)		62038.48	$8.90\ 10^{-10}$	(11, 10)→(9, 9)	257.65	1650860	$1.95\ 10^{-8}$
(4, 3)→(2, 2)	38.76	508996.1	$3.83\ 10^{-9}$	(11, 10)→(9, 10)		1711982	$9.67\ 10^{-8}$
(4, 3)→(2, 3)		566896.1	$3.21\ 10^{-8}$	(11, 11)→(9, 10)	260.42	1769632	$2.66\ 10^{-8}$
(4, 4)→(2, 3)	41.68	627757.3	$1.05\ 10^{-8}$	(11, 11)→(11, 12)		61725.07	$9.36\ 10^{-10}$
(4, 4)→(4, 5)		59233.57	$8.09\ 10^{-10}$	(11, 11)→(11, 10)		57649.32	$7.62\ 10^{-10}$
(4, 4)→(4, 3)		60861.17	$8.07\ 10^{-10}$	(12, 11)→(10, 10)	304.52	1813619	$2.20\ 10^{-8}$
(5, 4)→(3, 3)	58.33	672530.3	$6.00\ 10^{-9}$	(12, 11)→(10, 11)		1875048	$1.07\ 10^{-7}$
(5, 4)→(3, 4)		731187.3	$4.14\ 10^{-8}$	(12, 12)→(10, 11)	307.27	1932393	$2.92\ 10^{-8}$
(5, 5)→(3, 4)	61.22	79129.8	$1.28\ 10^{-8}$	(12, 12)→(12, 13)		62013.09	$9.43\ 10^{-10}$
(5, 5)→(5, 6)		59689.56	$8.35\ 10^{-10}$	(12, 12)→(12, 11)		57344.83	$7.45\ 10^{-10}$
(5, 5)→(5, 4)		60105.58	$8.47\ 10^{-10}$	(13, 12)→(11, 11)	355.28	1976296	$2.41\ 10^{-8}$
(6, 5)→(4, 4)	81.80	835848.2	$8.22\ 10^{-9}$	(13, 12)→(11, 12)		2038021	$1.15\ 10^{-7}$
(6, 5)→(4, 5)		895071.9	$5.07\ 10^{-8}$	(13, 13)→(11, 12)	358.02	2095072	$3.12\ 10^{-8}$
(6, 6)→(4, 5)	84.66	954611.3	$1.51\ 10^{-8}$	(13, 13)→(13, 14)		62294.66	$9.62\ 10^{-10}$
(6, 6)→(6, 7)		60095.03	$8.57\ 10^{-10}$	(13, 13)→(13, 12)		57050.94	$7.39\ 10^{-10}$
(6, 6)→(6, 5)		59539.44	$8.30\ 10^{-10}$	(14, 13)→(12, 12)	409.94	2138887	$2.65\ 10^{-8}$
(7, 6)→(5, 5)	109.17	999030.3	$1.05\ 10^{-8}$	(14, 13)→(12, 13)		2200900	$1.25\ 10^{-7}$
(7, 6)→(5, 6)		1058720	$5.99\ 10^{-8}$	(14, 14)→(12, 13)	412.66	2257665	$3.36\ 10^{-8}$
(7, 7)→(5, 6)	112.01	1117795	$1.74\ 10^{-8}$	(14, 14)→(14, 15)		62571.21	$9.63\ 10^{-10}$
(7, 7)→(7, 8)		60461.41	$8.75\ 10^{-10}$	(14, 14)→(14, 13)		56765.59	$7.19\ 10^{-10}$
(7, 7)→(7, 6)		59074.69	$8.14\ 10^{-10}$	(15, 14)→(13, 13)	468.48	2301387	$2.86\ 10^{-8}$
(8, 7)→(6, 6)	140.44	1162112	$1.29\ 10^{-8}$	(15, 14)→(13, 14)		2363682	$1.33\ 10^{-7}$
(8, 7)→(6, 7)		1222207	$7.04\ 10^{-8}$	(15, 15)→(13, 14)	471.20	2420169	$3.58\ 10^{-8}$
(8, 8)→(6, 7)	143.26	1280877	$2.02\ 10^{-8}$	(15, 15)→(15, 16)		62843.36	$9.89\ 10^{-10}$
(8, 8)→(8, 9)		60801.16	$8.92\ 10^{-10}$	(15, 15)→(15, 14)		56486.91	$7.18\ 10^{-10}$
(8, 8)→(8, 7)		58670.66	$8.00\ 10^{-10}$				

of 10 for C and O and a depletion of 10^4 for sulfur and metals (i.e. H:He:C:O:S:Mg:Fe:Si = 1:0.098:3.8 10^{-5}:8.5 10^{-5}: 1.6 $^{-9}$:3.8 10^{-9}:4.7 10^{-9}:3.5 10^{-9}). As the abundance of $^{16}O^{18}O$ is quite similar to the one of $^{16}O_2$ divided by 250, we do not present it here, the interested reader can find the information in MVB. We will only present here the emissivities of $^{16}O^{18}O$ (expressed in mK km s^{-1}) as a function of some selected cloud parameters.

Our model allows to compute the emissivity of the 71 $^{16}O^{18}O$ rotational lines taken into account in the model. Following what has been done for the rotational excitation of $^{16}O_2$ (MVB), the $^{16}O^{18}O$ line emissivities have been computed for different kinds of interstellar clouds and several parameters characterizing these clouds and their environment. We only present here the results obtained for the lines which are accessible from the ground. The most intense transition of $^{16}O^{18}O$ is the 119 GHz (N, J):(1, 1)–(1, 0) line as for $^{16}O_2$ but this frequency is strongly blocked by the telluric $^{16}O_2$ line. The most intense transitions of $^{16}O^{18}O$ which are accessible by ground-based telescopes are the 234 GHz (2, 1)–(0, 1), 298 GHz (2, 2)–(0, 1) and 402 GHz (3, 2)–(1, 2) lines for which receivers exist.

Fig. 1 displays the predicted emissivities of the 234, 298 and 402 GHz $^{16}O^{18}O$ lines versus the visual extinction for various values of the hydrogen density. The temperature distributions are obtained from the thermal balance equation. The temperature distribution throughout the cloud varies from cloud to cloud according to the total visual extinction and the density: it decreases with increasing A_V and n_H. Typically for n_H=500 cm^{-3}, the temperature decreases from 56 K at the edge of the cloud to 17 K in the core; for the densest clouds considerated here, with n_H=10^5 cm^{-3}, the temperature ranges from 32 K to 8 K. It can be noted that the 234 GHz line is the most intense one which could be observed by ground-based telescopes. This

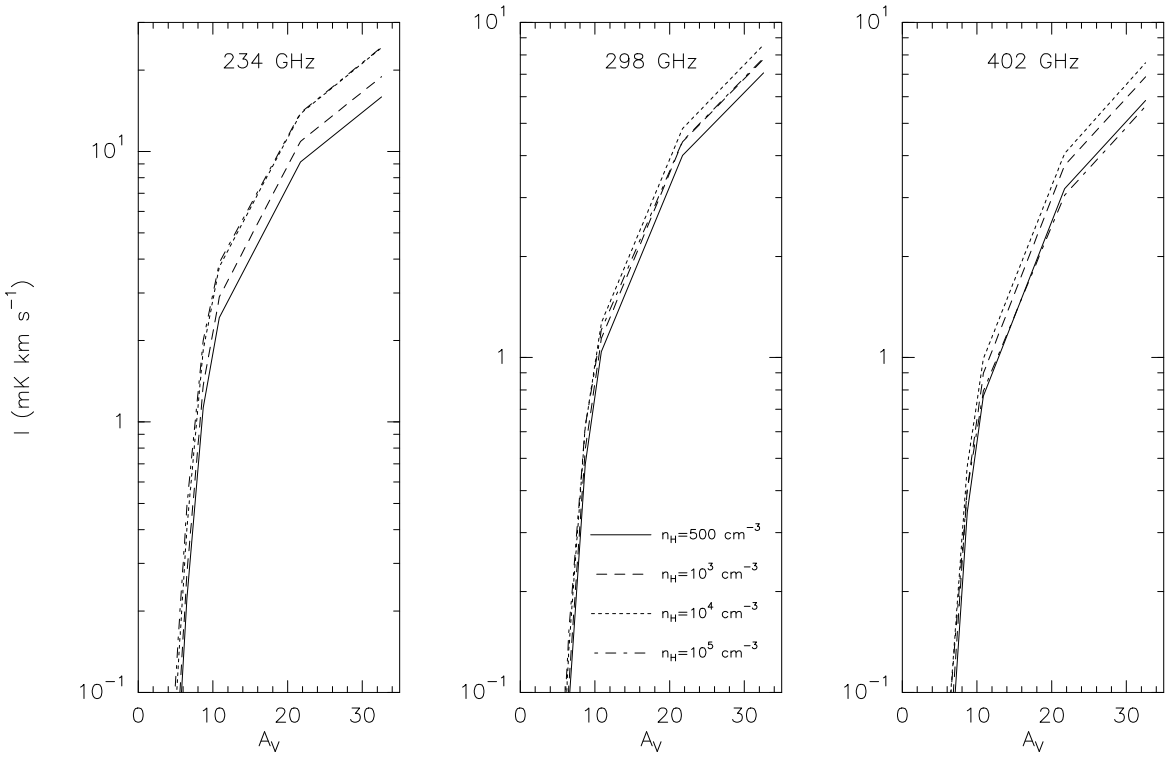

Fig. 1. Emissivities of $^{16}O^{18}O$ lines as a function of the total visual extinction throughout different kinds of clouds and as a function of hydrogen density n_H. Temperature distributions throughout the clouds are computed by solving the thermal balance equation.

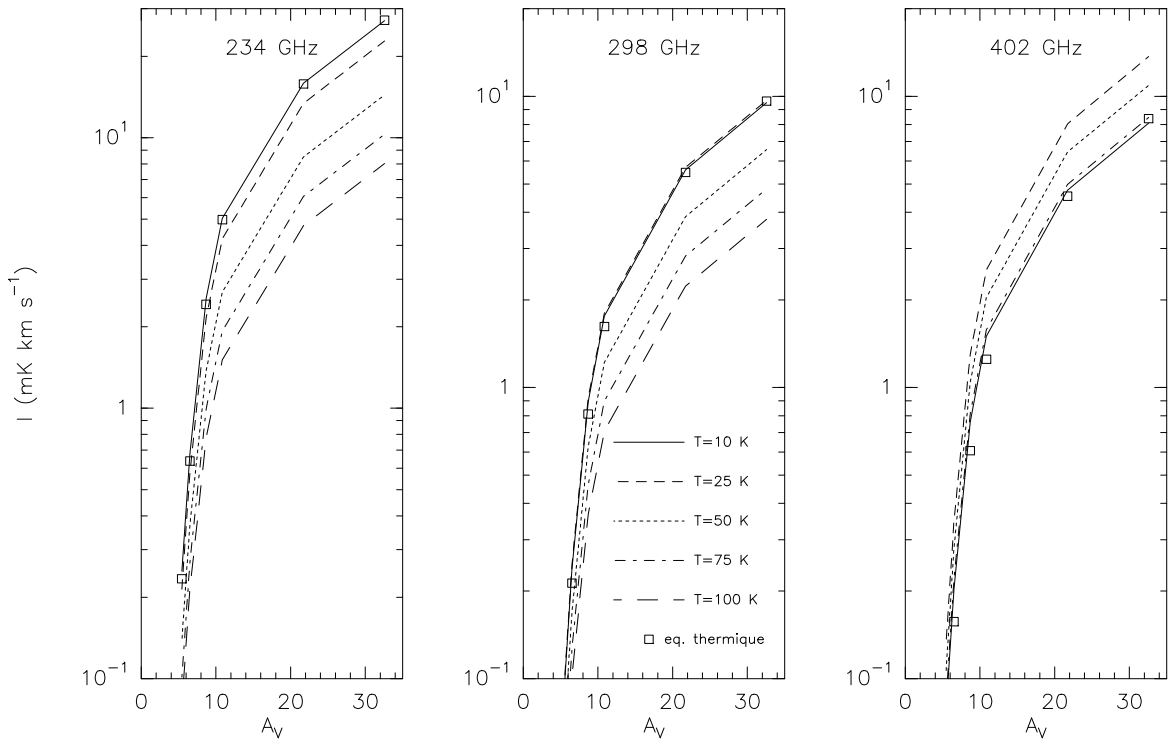

Fig. 2. Emissivities of $^{16}O^{18}O$ lines as a function of the total visual extinction throughout different kinds of clouds and as a function of temperature for clouds with n_H=10^4 cm^{-3}

is fortunate as it is also the easiest one to observe in terms of receiver sensitivity and atmospheric transparency.

The second series of models represents clouds with uniform temperature from T = 10 up to 100 K and n_H=10^4 cm^{-3}. Fig. 2 displays the emissivities of the 234, 298 and 402 GHz lines versus the visual extinction. Unlike the $^{16}O^{18}O$ abundance, the line intensities, controlled by the rotational population, are really sensitive to the temperature. Our model calculations show that the rotational population of $^{16}O^{18}O$ is close to LTE in opaque clouds ($A_V \geq$ 10–20) where lines have the best chance to be detected. In all situations, the (2, 1)–(0, 1) 234 GHz is more intense than the (2, 2)–(0, 1) 298 GHz and the (3, 2)–(1, 2) 402 GHz lines.

In the third series of models, the incident ultraviolet radiation field has been multiplied by a scaling factor f_{UV}=10, 100 and 10^3 to take into account molecular clouds near HII regions. All cloud models were run with n_H=10^4 cm^{-3} and T=10 K and the emissivities of the 234, 298 and 402 GHz lines are plotted in Fig. 3. The global decrease of the intensities is due to the decrease of abundance of $^{16}O^{18}O$ which is more efficiently destroyed when the UV field is stronger. For a same visual extinction, the UV radiation field is a determinant parameter for the emissivity of the $^{16}O^{18}O$ lines until the visual extinction becomes large enough ($A_V > 20$) to attenuate its effect. Typically, even for a cloud with an opacity as large as $A_V \sim$20, the emissivities are divided by 4 as f_{UV} increases from 1 to 10^3, implying a factor of 16 increase of the required integration time for a given receiver. With the present status of mm receivers, detection of $^{16}O^{18}O$ appears completely excluded in molecular clouds where massive star formation occurs.

Finally, the last two series of models check the influence of the C/O ratio on $^{16}O^{18}O$ detectability. We have computed two series of models with C/O=0.1, 0.4 and 0.7, one series with a constant carbon abundance X_C=3.8 10^{-5} and the other one with the oxygen abundance fixed to X_O=8.5 10^{-5}. All models are run with T=10 K and n_H=10^4 cm^{-3}. Figs. 4 and 5 display the predicted emissivities of the $^{16}O^{18}O$ lines at 234, 298 and 402 GHz versus the visual extinction for the two series of models. The C/O ratio is a dramatic parameter for the abundance and, consequently, for the emissivities of the $^{16}O^{18}O$ lines: when X_O is divided by 7 (Fig. 4) while the carbon abundance remains constant, the emissivities decrease by a factor of about 40. When the oxygen abundance is constant and X_C is increased by a factor of 7 (Fig. 5), the emissivities decrease by a factor of about 10. This means an increase of the integration time for a given receiver by a factor 1600 and 100, respectively. With the sensitivities of present receivers, $^{16}O^{18}O$ could only be detected if the C/O ratio is lower or of the same order than the "standard" cosmic value (C/O$\sim$0.4).

For nearly all the different sets of parameters presented in this section, the intensity of the 234 GHz is from 2 to 4 times higher than that of the 298 and 402 GHz lines. As the 234 GHz line has not been detected, detections of the two other lines seem presently unrealistic.

4. Comparison with the observations

The observations of the 234 GHz line of $^{16}O^{18}O$ have been made during four consecutive winters at POM-2 telescope from December 1992 to January 1996 and have been presented in Pagani et al. (1993) and MPLC. The sources are four cold, dark molecular clouds (T_{kin} $\sim$10 K): B5, TMC2, L134N and B335, three lukewarm clouds (T_{kin} $\sim$20 K): OMC3, NGC2264(IRS2) and DR21, and one warm cloud (T_{kin} $\sim$40 K): NGC7538.

As the line has not been detected in any of the observed clouds except for one possible case, namely L134N (0', 0') for which we can get a tentative value, only upper limits of the $^{16}O^{18}O$ column densities have been derived. To analyse the observations, we have performed model calculations of the observed clouds. In cloud modeling, an important free parameter is the visual extinction A_V throughout the cloud; this parameter is correlated with the H_2 column densities. Since CO is a good tracer of H_2 in the interstellar medium, we have deduced the H_2 column densities of the observed clouds from those of $C^{18}O$ using the relation derived by Frerking et al. (1982) in the Taurus region:

$$N(\mathrm{H_2}) = \left[N(\mathrm{C^{18}O})/1.7\ 10^{14} + 1.3\right] 10^{21}\ \mathrm{cm^{-2}}$$

$$\text{for } N(\mathrm{C^{18}O}) > 3\ 10^{14}\ \mathrm{cm^{-2}} \qquad (3)$$

Fig. 6 shows the $^{16}O^{18}O$ column density as a function of the H_2 column density throughout the cloud computed for several series of homogeneous steady state models (this work) as well as for four fragmented cloud models developed by Spaans (private communication). The upper limits of the $^{16}O^{18}O$ column densities derived for the eight clouds observed by MPLC are also plotted in Fig. 6. As the hydrogen density and the temperature do not affect the column density of the molecular oxygen in the ranges 500$\leq n_H \leq$$10^5$ cm^{-3} and 10$\leq T \leq$100 K, all models represented in Fig. 6 have the same density n_H = 10^4 cm^{-3} and the same temperature T = 10 K. The full line on Fig. 6 represents "standard" models with C/O = 0.4 (X_C = 3.6 10^{-5}, X_O = 8.5 10^{-5}) and f_{UV} = 1. We have also performed calculations by varying only one parameter with respect to the standard model: The long dashed curve displays results obtained in an enhanced UV field, with f_{UV} = 1000; the dotted and dash dotted curves display results obtained for an enhanced C/O ratio of 0.7 with X_C and X_O kept constant, respectively.

One can see that, for half of the observed clouds (NGC2264(IRS2), DR21, OMC3, L134N (4', -1') and TMC2), the upper limits of the column densities obtained for $^{16}O^{18}O$ are significantly lower than the column densities computed with standard conditions. The model overestimates the amount of $^{16}O^{18}O$ by factors between 2 and 10 if the true column densities are near the derived upper limits. The discrepancy can be much larger if the true column densities are well below, indicating a clear problem for the standard O_2 chemistry.

An increase of the ultraviolet radiation field could be compatible with the low column densities of $^{16}O^{18}O$ derived for L134N and TMC2. However, it cannot explain the results for NGC2264(IRS2), DR21 and OMC3. Furthermore, all sources

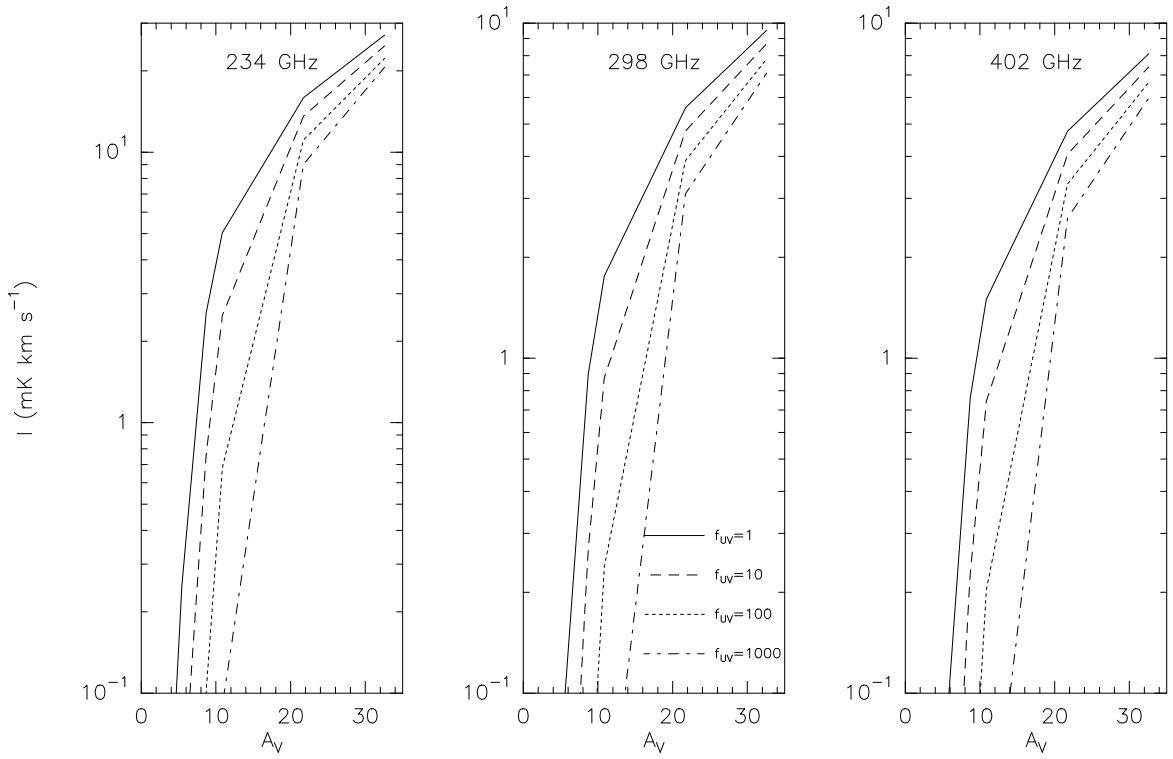

Fig. 3. Emissivities of $^{16}O^{18}O$ lines as a function of the total visual extinction throughout different kinds of clouds and UV radiation field for clouds with n_H=10^4 cm^{-3} and T=10 K

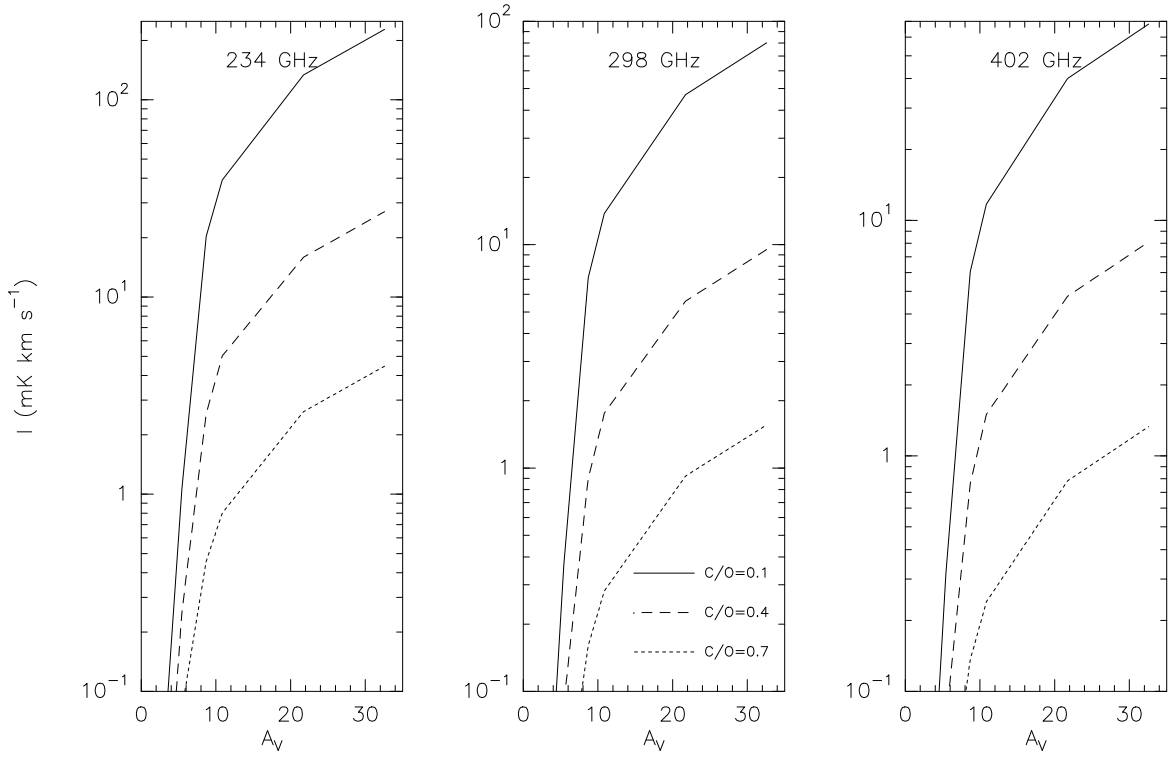

Fig. 4. Emissivities of $^{16}O^{18}O$ lines as a function of the total visual extinction throughout different kinds of clouds and as a function of C/O ratio for isothermal clouds (n_H=10^4 cm^{-3} and T=10 K). The fractional abundance of carbon is constant: X_C=3.8 10^{-5}

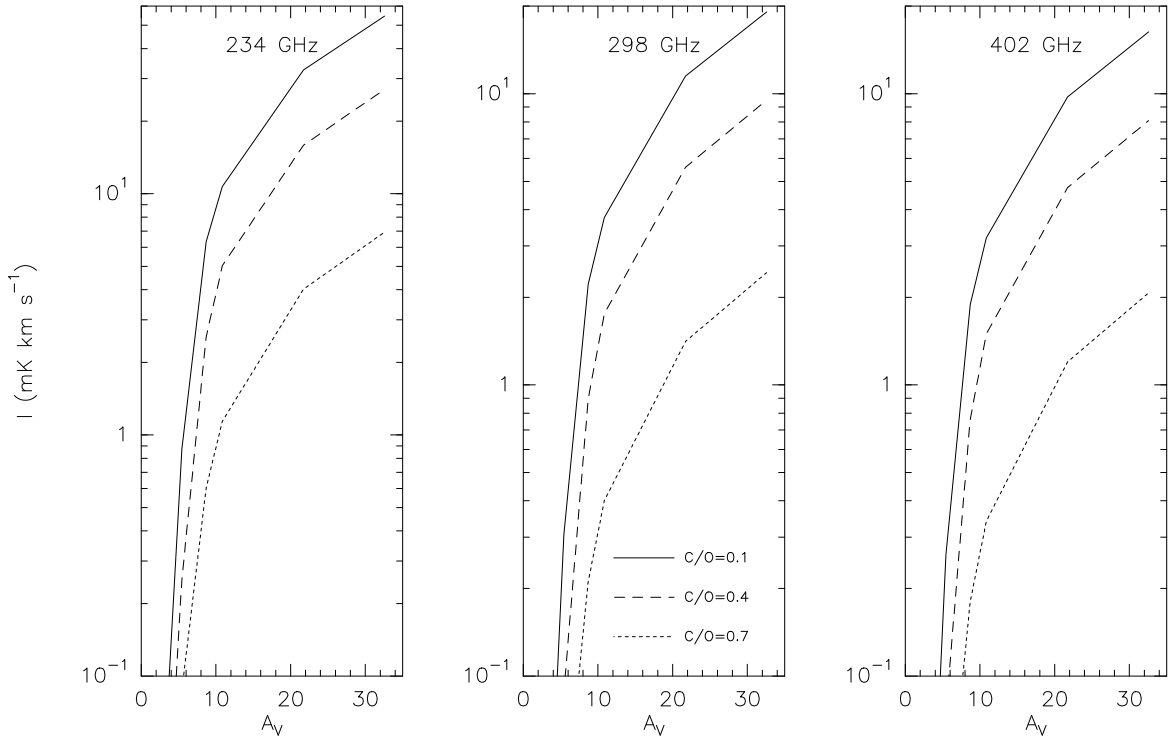

Fig. 5. Emissivities of $^{16}O^{18}O$ lines as a function of the total visual extinction througout different kinds of clouds and as a function of C/O ratio for isothermal clouds (n_H=10^4 cm^{-3} and T=10 K). The fractional abundance of oxygen is constante: X_O=8.5 10^{-5},

have been chosen without intense UV radiation field on the scale of the beamsize, so that it is difficult to emphasize a high UV radiation field to explain the observations of these three clouds.

As the C/O elemental ratio plays a dominant role on the abundance of molecular oxygen and the emissivities of its rotational lines (see discussion of MVB), an increase of the C/O ratio in the gaseous phase with respect to its "standard" value can account for the underabundance of $^{16}O^{18}O$. Fig. 6 shows that C/O $\geq$ 0.7 makes the model compatible with the observed upper limits of $N(^{16}O^{18}O)$.

The case of L134N (0', 0'), if real, is clearly atypical because it stands above the "standard" model (Fig. 6) and thus requires a C/O ratio between 0.1 and 0.4. Because L134N is considered to be a peculiar oxygen-rich cloud, there is a real possibility to find anomalous oxygen abundance at this place and nowhere else. Indeed each observed molecule traces a different volume which means that the chemistry is highly inhomogeneous (Swade 1989). On top of that, the case seems to be stronger now as a recent paper (Stark at al. 1996) has shown that in that direction two CI lines could be seen, a main one at the bulk gas velocity (2.5 km/s) and a satellite line at $\sim$1.3 km/s which corresponds to our third $^{16}O^{18}O$ component towards that position (Pagani et al. 1993). Thus all three lines could be $^{16}O^{18}O$ features. If true the chemistry and/or excitation of molecular oxygen in this cloud is a complete puzzle still to be elucidated.

In the general case of non-detection, the variation of the C/O ratio is not the only possible explanation to the low abundance of $^{16}O^{18}O$ in molecular clouds. An efficient destruction of molecular oxygen can occur if the cloud is clumpy because the UV photons can penetrate deeper into the cloud. This effect is illustrated in Fig. 6, in which we have included the four $^{16}O^{18}O$ column densities computed from the inhomogeneous model of Spaans (private communication) for different clump volume filling factors (F). In these models, F varies from 10 to 50 %, the clump-interclump density ratio is 30 and the clump size is 0.1 pc. Though strong observational evidences of the clumpiness of the interstellar clouds exist, they are still qualitative and do not allow to estimate the filling factor, the density ratio or the clump size. The clumpiness of the clouds could be a good way to reduce the discrepancy between theory and observations. In some cases however, it does not appear sufficient to explain some low values of the molecular oxygen abundance. For instance, the upper limit upon $N(^{16}O^{18}O)$ for NGC2264(IRS2) still remains a factor of 2 lower than the value expected with a low filling factor (10 %).

To conclude this section, let us point out the main uncertaintly on our model calculations: the collisional excitation $^{16}O^{18}O$ is rather uncertain. If extrapolation of collisional rates (see appendix) from the main isotope can be warranted, in the first approximation, for collisions between odd-odd N levels or even-even N levels, it is more questionable for collisions between odd N and even N levels, i.e. for ΔN=1, 3, 5... The possibility that these rates are much smaller than the ones corresponding to even ΔN can not be excluded. To check this, we have run a "standard" cloud model ($A_V\sim$11, $n_{\rm H}$=10^4 cm^{-3} and T=10 K) with the collisional rates for odd ΔN reduced by

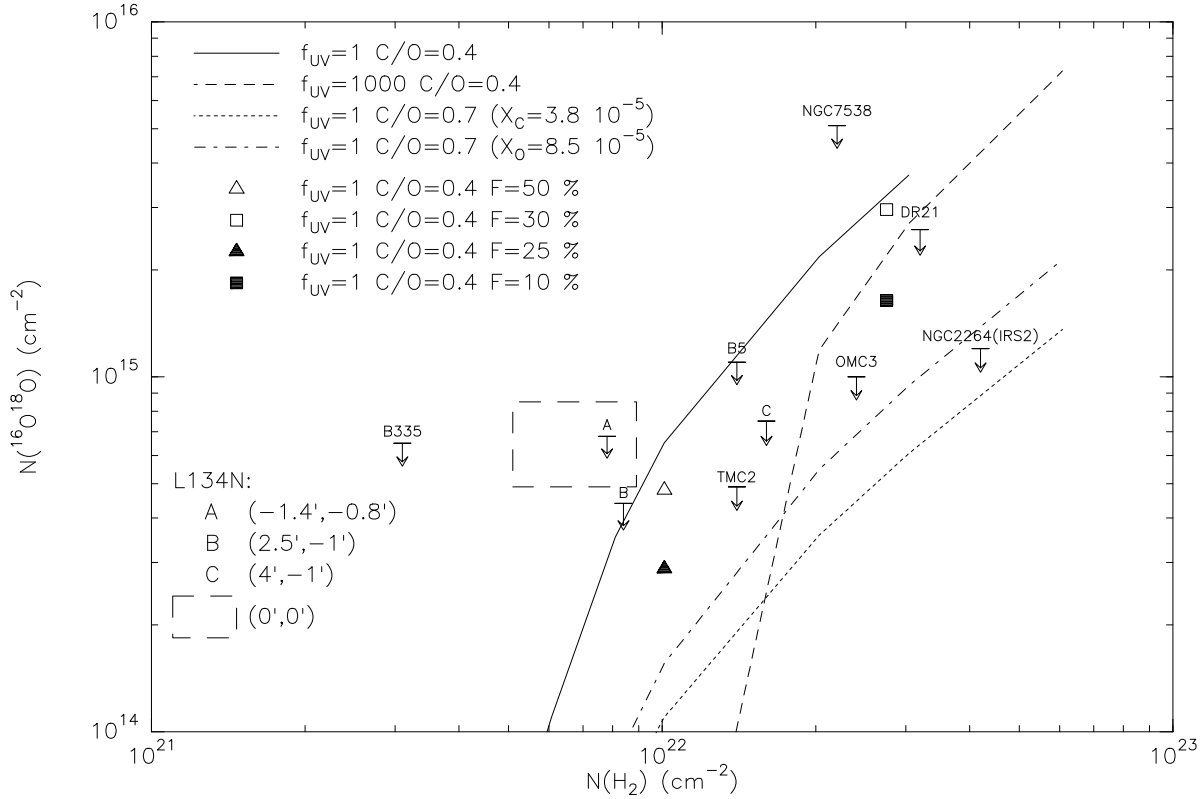

Fig. 6. $N(^{16}O^{18}O)$ as a function of $N(H_2)$: All models have the same temperature T=10 K and hydrogen density n_H=10^4 cm^{-3}. The points represent the inhomogeneous model of Spaans for various clump volume filling factors (F), the triangles and squares simply represent two differents H_2 column densities of $N(H_2)$=10^{22} cm^{-2} and $N(H_2)$=2.8 10^{22} cm^{-2} respectively. The rectangle represents the possible region of $N(^{16}O^{18}O)$ for our tentative detection in L134N. Horizontal box sides represent $\pm 1\sigma$ values while vertical box sides represent the minimum and maximum $N(C^{18}O)$ (see Pagani et al. 1993).

a factor 100 with respect to the ones tabulated in Table 4. Table 3 gives the population of the first sixteen levels of $^{16}O^{18}O$ and the emissivities of the 234, 298 and 402 GHz lines obtained with the normal odd ΔN collisional rates and rates reduced by a factor 100. Differences between the two series of calculations are very small and never exceed 10 %, indicating that collisions with odd ΔN have little influence on the $^{16}O^{18}O$ rotational population, at least for the physical conditions prevailing in dense dark clouds.

5. The isotopic ratio $^{16}O/^{18}O$

Taking into account the chemistry of ^{13}C and ^{18}O bearing species, our model allows to compute the isotopic abundance ratio of oxygen-bearing species, $X^{16}O/X^{18}O$, and to determine whether isotopic fractionation occurs for some of them, and in particular for O_2.

This is illustrated in Fig. 7 for the oxygen-bearing species O, CO, O_2, OH and H_2O where are plotted the normalized column density ratios R defined by:

$$R\left(X^{16}O/X^{18}O\right) = \frac{N(X^{16}O)/N(X^{18}O)}{[^{16}O]/[^{18}O]} \quad (4)$$

except for O_2 where:

$$R\left(O_2/^{16}O^{18}O\right) = 2\,\frac{N(O_2)/N(^{16}O^{18}O)}{[^{16}O]/[^{18}O]} \quad (5)$$

The ratio $R(X^{16}O/X^{18}O)$ should be about 1 if there is no isotopic fractionation. The effect of the selective photodissociation of CO and its isotopic variants on the $C^{16}O/C^{18}O$ ratio in interstellar clouds has already been studied by several authors (Bally & Langer 1982, Chu & Watson 1983, Glassgold et al. 1985, Warin et al. 1996). It is briefly recalled here: for very low visual extinctions, there is no efficient protection against the ultraviolet radiation field and the photo-destruction rates of CO and $C^{18}O$ are similar, so that $R(CO/C^{18}O)$ is close to unity. As the visual extinction increases, CO protects itself more efficiently than $C^{18}O$ because of its larger abundance, so that $R(CO/C^{18}O)$ increases. The maximum enhancement occurs for A_V = 2–4 and increases with increasing density as a consequence of a more efficient CO formation. When the UV radiation field becomes too attenuated to photodissociate CO or $C^{18}O$, $R(CO/C^{18}O)$ decreases back to unity ($A_V \sim 7$) and becomes constant again. The photodissociation of the other oxygen-bearing species occurs through a continuum, so that selective photo-dissociation does not occur for these species. For

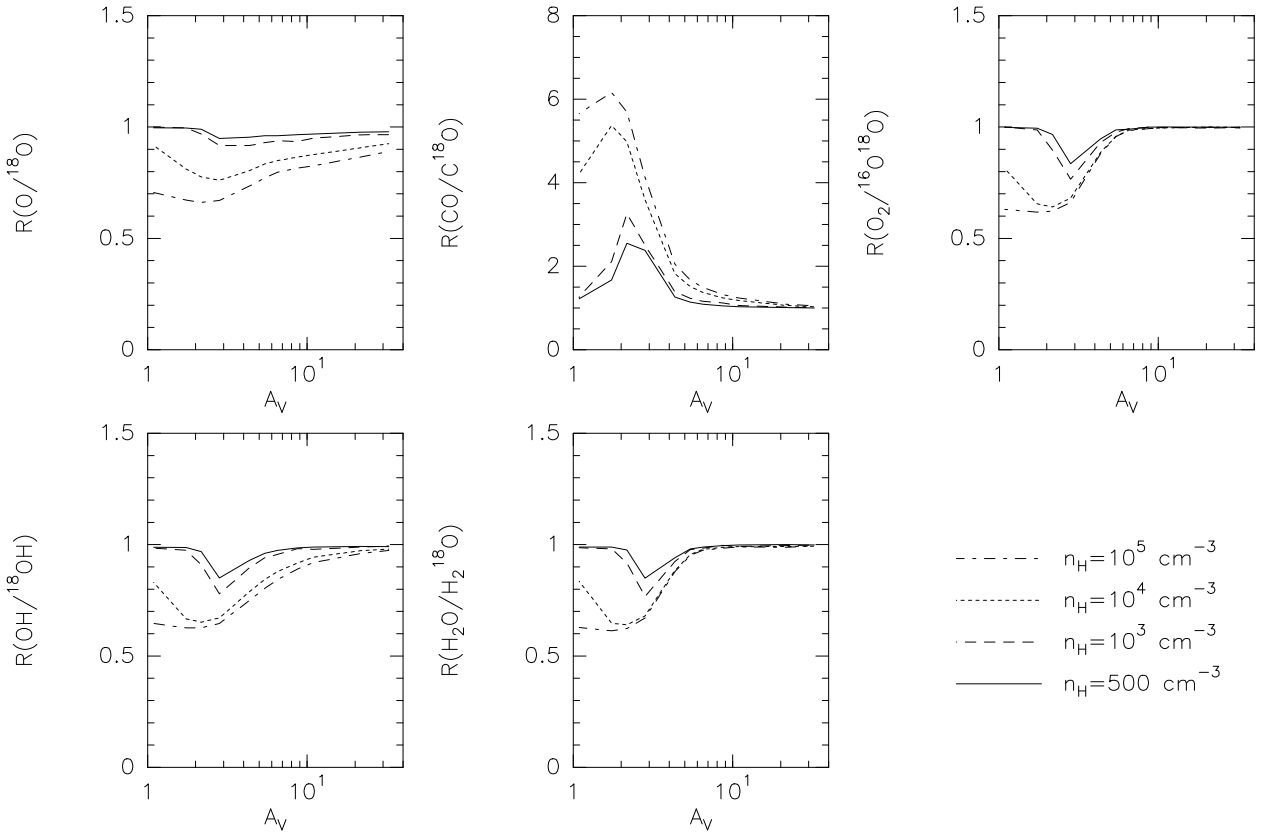

Fig. 7. The influence of the isotopic fractionation on the column densities of the principal oxygen-bearing species for cloud models at thermal equilibrium

the three other oxygenated molecules included in the model: OH, H_2O and O_2 the normalized column density ratio is anti-correlated with that of CO: it decreases and reaches a minimum for A_V = 2–4. In this region, where R(CO/C^{18}O) is higher than unity, C^{18}O is more easily photodissociated than CO and the medium is enriched into ^{18}O, which allows a larger formation of the other ^{18}O-substituted molecules to occur.

Isotopic fractionation does not affect dark clouds, where O_2 has a better chance to be detected, so that the low value of ^{16}O^{18}O abundance derived from the observations also indicates a low abundance for the main isotope. The effect of isotopic fractionation must be taken into account in diffuse and translucent clouds. When the fractionation is maximum, neglecting the isotopic fractionation may let one underestimate the CO column density by a factor of 6 and overevaluate the abundance of other oxygen-bearing species by a factor of 2.5 if the column densities of the main isotopes are deduced from the observations of the ^{18}O-bearing species. For the O_2/CO ratio, the overestimate can reach a factor of 15 for $A_V \sim 2$ but this has no consequence since O_2 should be undetectable in such clouds.

6. Discussion and conclusion

Except possibly in one single case, L134N (0, 0), no detection of ^{16}O^{18}O has been obtained up to now and the low abundance of ^{16}O^{18}O obtained by MPLC seems to reveal a general characteristic of dark clouds. For half of the observed clouds: NGC2264(IRS2), DR21, OMC3, L134N (4', -1') and TMC2, the low upper limits of the column densities obtained for ^{16}O^{18}O are significantly lower than the column densities computed with standard conditions. Our cloud model allows to explain this underabundance of molecular oxygen by an increase of the C/O elemental ratio in the gas phase with respect to the cosmic value. This decrease by a factor of 2 of the oxygen available in the gaseous phase could be due to a selective depletion of oxygen on grain ice mantles under the form of H_2O, CO, CO_2 and O_2 (Langer et al. 1984, Blake et al. 1987). To constrain the elemental abundances in the gas phase and, particularly the oxygen one, Ehrenfreud et al. (1992) suggest the possibility of observing solid O_2 and other compounds of the interstellar mantle ices with ISO. An increase of the C/O ratio is among the simplest explanations, to which it is often referred. Whether it has some reality and is not an "ad hoc" hypothesis could be checked by comparing computed and observed abundances of several chemical species sensitive to this C/O ratio. This is planned for the future.

Another explanation could help us to understand the low abundance of molecular oxygen. A higher ionisation degree than the one obtained in most of the chemical models leads to a more efficient destruction of O_2 and ^{16}O^{18}O. This ionisa-

Table 3. Population of the first sixteen rotational levels of $^{16}O^{18}O$ and emissivities of the 234, 298 and 402 GHz lines in a "standard" dark cloud ($A_V \sim 11$, $n_H = 10^4$ cm^{-3} and $T = 10$ K) for two series of collisional rates: the one tabulated in Table 4 (Rates 1) and those with the odd ΔN rates reduced by a factor 100 (Rates 2).

	Rates 1	Rates 2
N($^{16}O^{18}O$(N=0, J=1))/N($^{16}O^{18}O$)	0.19	0.19
N($^{16}O^{18}O$(N=1, J=0))/N($^{16}O^{18}O$)	0.059	0.061
N($^{16}O^{18}O$(N=1, J=2))/N($^{16}O^{18}O$)	0.22	0.22
N($^{16}O^{18}O$(N=1, J=1))/N($^{16}O^{18}O$)	0.11	0.10
N($^{16}O^{18}O$(N=2, J=1))/N($^{16}O^{18}O$)	0.061	0.058
N($^{16}O^{18}O$(N=2, J=3))/N($^{16}O^{18}O$)	0.13	0.14
N($^{16}O^{18}O$(N=2, J=2))/N($^{16}O^{18}O$)	0.078	0.074
N($^{16}O^{18}O$(N=3, J=2))/N($^{16}O^{18}O$)	0.030	0.029
N($^{16}O^{18}O$(N=3, J=4))/N($^{16}O^{18}O$)	0.052	0.054
N($^{16}O^{18}O$(N=3, J=3))/N($^{16}O^{18}O$)	0.033	0.031
N($^{16}O^{18}O$(N=4, J=3))/N($^{16}O^{18}O$)	0.0087	0.0080
N($^{16}O^{18}O$(N=4, J=5))/N($^{16}O^{18}O$)	0.013	0.014
N($^{16}O^{18}O$(N=4, J=4))/N($^{16}O^{18}O$)	0.0083	0.0087
N($^{16}O^{18}O$(N=5, J=4))/N($^{16}O^{18}O$)	0.0087	0.0083
N($^{16}O^{18}O$(N=5, J=6))/N($^{16}O^{18}O$)	0.0016	0.0014
N($^{16}O^{18}O$(N=5, J=5))/N($^{16}O^{18}O$)	0.0022	0.0023
$^{16}O^{18}O$:(2, 1)→(0, 1) 234 GHz (mK.km.s^{-1})	5.03	4.80
$^{16}O^{18}O$:(2, 2)→(0, 1) 298 GHz (mK.km.s^{-1})	1.76	1.66
$^{16}O^{18}O$:(3, 2)→(1, 2) 402 GHz (mK.km.s^{-1})	1.50	1.44

tion can be obtained in the phase called "HIP" (High Ionization Phase) of the models of Le Bourlot et al. (1995) which show the possible existence of two stable phases in the chemical composition of interstellar clouds with a high ionization degree and a low one. Another hypothesis (Pineau des Forêts et al. 1992, Xie et al. 1995) suggests a mixing between the core and the edges of the cloud, which could be caused by turbulence and which should increase the C^+ abundance in the cloud core leading to an efficient destruction of O_2 and $^{16}O^{18}O$.

If one could hope to detect the 234 GHz line of $^{16}O^{18}O$ in molecular clouds, the introduction of $^{16}O^{18}O$ rotational excitation in our model clearly shows that the detection of this molecule at other frequencies (e.g. 298 and 402 GHz) is unrealistic at the moment with present millimeter receivers. Spectroscopic parameters and collisional excitation rates of $^{16}O^{18}O$ by He derived in this work allow to perform model calculations of the excitation of this molecule in other astrophysical environments (circumstellar envelopes, photodissociation regions...).

The explicit treatment of the ^{18}O chemistry shows that the selective photo-dissociation of CO and $C^{18}O$ does not only affect the ratio of these two molecules but also all the oxygen-bearing species in diffuse and translucent clouds. Thus, in such clouds, the use of the standard isotopic ratio [^{16}O]/[^{18}O] could be dangerous to determine the abundance of oxygen-bearing species from the observations of their isotopic substitutes even if these species do not have any selective photodissociation. In dark clouds, however there is no isotopic fractionation for the ^{18}O substitutes included in the model: the low $^{16}O^{18}O$ abundance indicates a low abundance of the main isotope O_2.

Acknowledgements. Model calculations have been performed on the computers of the Service Informatique de l'Observatoire de Paris. We would like to thank M. Spaans who supplied us with his model results and for helpful discussions.

Appendix A: collision rates $^{16}O^{18}O$–He

To obtain the de-excitation rates of $^{16}O^{18}O$–He, the collisional transitions are separated into 9 groups:

1) $J = N - 1$, $J' = N' - 1$ 2) $J = N - 1$, $J' = N'$
3) $J = N - 1$, $J' = N' + 1$ 4) $J = N$, $J' = N' - 1$
5) $J = N$, $J' = N'$ 6) $J = N$, $J' = N' + 1$
7) $J = N + 1$, $J' = N' - 1$ 8) $J = N + 1$, $J' = N'$
9) $J = N + 1$, $J' = N' + 1$

For each group, N indicates the initial level, N', the final one and $\Delta N = N - N'$ and we have used the following hypothesis to obtained the de-excitation rates:

- For odd values of N and N', the rates are equal to those of O_2.
- For odd values of N and even values of N', the rates are obtained by averaging the rates of the transition $N \rightarrow N' - 1$ and the transition $N \rightarrow N' + 1$. For odd values of N and (N'=0, J'=1), the rates are obtained by extrapolation from all the rates from the same N to $N' \neq 0$.
- For even values of N and N' (even values of ΔN), the rates are obtained by averaging the rates of N-1 and N+1 (equal to those of O_2) for the same value of ΔN. For even values of N and (N'=0, J'=1), the rates are obtained by extrapolation from all the rates with the same value of ΔN and $N' \neq 0$.
- For even values of N and odd values of N', the rates are obtained by averaging the rates of the transition $N - 1 \rightarrow N'$ and transition $N + 1 \rightarrow N'$.

The excitation rates are obtained by the usual reversibility law and the collisional rates of $^{16}O^{18}O$–H_2 are equal to those of $^{16}O^{18}O$–He multiplied by the reduced mass factor $\sqrt{\mu_{He}/\mu_{H_2}} \sim \sqrt{2}$ (see MVB).

References

Anicich V.G., 1993, J. Chem. Ref. Data 22, 1469
Anders E., Grevesse N., 1989, Geochimica et Cosmochimica Acta 53, 197
Bally J., Langer W.D., 1982, ApJ 255, 143
Blake G. A., Sutton E. C., Masson C. R., Phillips T. G., 1987, ApJ 315, 621
Chièze J.P., Pineau des Forêts G., 1989, A&A 221, 89
Chu Y.H., Watson W.D., 1983, ApJ 267, 151
Combes F., Casoli F., Encrenaz P., Gerin M., Laurent C., 1991, A&A 298, 607
Combes F., Wiklind T., 1995, A&A 303, L61
Corey G.C., 1984, J. Chem. Phys. 81, 2678
Corey G.C., Alexander M.H., Schaefer J., 1986, J. Chem. Phys. 85, 2726

Davidsson J., Stenholm L.G., 1990, A&A 230, 504
Ehrenfreund P., Breukers R., d'Hendecourt L., Greenberg J.M., 1992, A&A 260, 431
Frerking M.A., Langer W.D., Wilson R.W., 1982, Apj 262, 590
Fuente A., Cernicharo J., Gracia-Burillo S., Tejero J., 1993, A&A 275, 558
Glassgold A.E., Huggins P.J., Langer W.D., 1985, ApJ 290, 615
Goldsmith P.F., Snell R.L., Erikson N.R., Dickman R.L., Scloerb F.P., Irvine W.M., 1985, ApJ 289, 613
Gordy W., Cook R.L., 1984, Microwave molecular spectra, Wiley Interscience Publication
Herbst E., Klemperer W., 1973, ApJ 185, 205
Langer W. D., Graedel T. E., Frerking M. A., Armentrout P. B., 1984, ApJ 277, 581
Le Bourlot J., Pineau des Forêts G., Roueff E., 1995, A&A 297, 251
Liszt H.S., Vanden Bout P.A., 1985, ApJ 291, 178
Maréchal P., Pagani L., Langer W.D., Castets A., 1997a, A&A 318, 252 (MPLC)
Maréchal P., Viala Y. P., Benayoun J. J., 1997b, A&A in press (MVB)
Mathis J.J., Mezger P.G., Panagia N., 1983, A&A 128, 212
Millar T.J., Farquhar P.R.A., Willacy K., 1996, A&AS in press
Orlikowsky T., 1986, Molecular Physics 56, 35
Pagani L., Langer W. D., Castets A., 1993, A&A 274, L13
Pineau des Forêts G., Flower D. R., Chieze J. P., 1992, MNRAS 256, 247
Spaans M., 1996, A&A 307, 271
Stark R., Wesselins P.R., van Dishoeck E.F., Laureys R.J., 1996, A&A 311, 282
Steinbach, 1974, PhD Thesis
Swade D.A.S., 1989, ApJ 345, 828
Viala Y.P., 1986, A&AS 64, 391
Viala Y.P., Walmsley C.M., 1976, A&A 50, 1
Warin S., Benayoun J.J., Viala Y.P., 1996, A&A 308, 535
Xie T., Allen M., Langer W. D., 1995, ApJ 440, 674

This article was processed by the author using Springer-Verlag LaTeX A&A style file *L-AA* version 3.